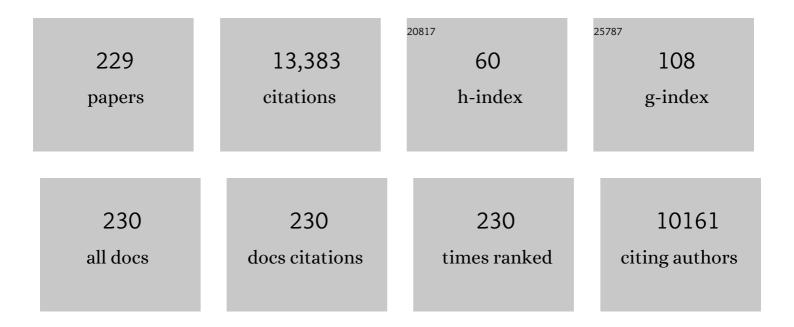
Changyu Shen

List of Publications by Year in descending order

Source: https://exaly.com/author-pdf/1893604/publications.pdf Version: 2024-02-01



#	Article	IF	CITATIONS
1	Nonisothermal melt and cold crystallization behaviors of biodegradable poly(lactic acid)/Ti3C2Tx MXene nanocomposites. Journal of Thermal Analysis and Calorimetry, 2022, 147, 2239-2251.	3.6	10
2	Simulation of Polymer Melt Injection Molding Filling Flow Based on an Improved SPH Method with Modified Lowâ€Ðissipation Riemann Solver. Macromolecular Theory and Simulations, 2022, 31, 2100029.	1.4	10
3	Electromagnetic interference shielding enhancement of poly(lactic acid)-based carbonaceous nanocomposites by poly(ethylene oxide)-assisted segregated structure: a comparative study of carbon nanotubes and graphene nanoplatelets. Advanced Composites and Hybrid Materials, 2022, 5, 209-219.	21.1	69
4	Fabrication of Polyether–Ether–Ketone Foams with Superior Properties and Mitigated Weld Lines by Microcellular Injection Molding. Advanced Engineering Materials, 2022, 24, 2100766.	3.5	5
5	Markedly improved hydrophobicity of cellulose film via a simple one-step aminosilane-assisted ball milling. Carbohydrate Polymers, 2022, 275, 118701.	10.2	13
6	Flexible layered cotton cellulose-based nanofibrous membranes for piezoelectric energy harvesting and self-powered sensing. Carbohydrate Polymers, 2022, 275, 118740.	10.2	16
7	Stretchable, Sensitive Strain Sensors with a Wide Workable Range and Low Detection Limit for Wearable Electronic Skins. ACS Applied Materials & Interfaces, 2022, 14, 4562-4570.	8.0	35
8	Facile preparation of a cellulose derived carbon/BN composite aerogel for superior electromagnetic wave absorption. Journal of Materials Chemistry C, 2022, 10, 5311-5320.	5.5	20
9	Ni Flower/MXene-Melamine Foam Derived 3D Magnetic/Conductive Networks for Ultra-Efficient Microwave Absorption and Infrared Stealth. Nano-Micro Letters, 2022, 14, 63.	27.0	108
10	Farmingâ€Inspired Continuous Fabrication of Grating Flexible Transparent Film with Anisotropic Conductivity. Advanced Materials Technologies, 2022, 7, .	5.8	4
11	Microspheres Modified with Superhydrophobic Nonâ€Woven Fabric with Highâ€Efficiency Oil–Water Separation: Controlled Water Content in PLA Solution. Macromolecular Materials and Engineering, 2022, 307, .	3.6	12
12	MXene/Polylactic Acid Fabric-Based Resonant Cavity for Realizing Simultaneous High-Performance Electromagnetic Interference (EMI) Shielding and Efficient Energy Harvesting. ACS Applied Materials & Interfaces, 2022, 14, 14607-14617.	8.0	17
13	Combined effect of poly(ethylene glycol) and boron nitride nanosheets on the crystallization behavior and thermal properties of poly(lactic acid). Journal of Thermal Analysis and Calorimetry, 2022, 147, 11147-11158.	3.6	2
14	Self-Reinforced Thermoplastic Polyurethane Wrinkled Foams with High Energy Absorption Realized by Gas Cooling Assisted Supercritical CO ₂ Foaming. Industrial & Engineering Chemistry Research, 2022, 61, 4832-4841.	3.7	3
15	Environmentâ€tolerant conductive and superhydrophobic poly(mâ€phenylene isophthalamide) fabric prepared via γâ€ray activation and reduced graphene oxide/nano <scp>SiO₂</scp> modification. Journal of Applied Polymer Science, 2022, 139, .	2.6	3
16	Hierarchical HCF@NC/Co Derived from Hollow Loofah Fiber Anchored with Metal–Organic Frameworks for Highly Efficient Microwave Absorption. ACS Applied Materials & Interfaces, 2022, 14, 2038-2050.	8.0	44
17	é«~è',åŧ速率的è€ç›ç»‡ç‰©åŸºå¨å®å€™å•用å‰çƒ-电çƒè',åŧ 器. Science China Materials, 2022, 65, 24	7 %2 490.	17

¹⁸ Impedance response behavior and mechanism study of axon-like ionic conductive cellulose-based hydrogel strain sensor. Advanced Composites and Hybrid Materials, 2022, 5, 1812-1820.

21.1 50

#	Article	IF	CITATIONS
19	Mechanically robust and conductive poly(acrylamide) nanocomposite hydrogel by the synergistic effect of vinyl hybrid silica nanoparticle and polypyrrole for human motion sensing. Advanced Composites and Hybrid Materials, 2022, 5, 2834-2846.	21.1	46
20	Graphene oxide/thermoplastic polyurethane wrinkled foams with enhanced compression performance fabricated by dynamic supercritical <scp>CO₂</scp> foaming. Journal of Applied Polymer Science, 2022, 139, .	2.6	8
21	Amino Termination of Ti ₃ C ₂ MXene Induces its Graphene Hybridized Film with Enhanced Ordered Nanostructure and Excellent Multiperformance. Advanced Materials Interfaces, 2022, 9, .	3.7	3
22	Crystallization Behavior of Rapid-Compression-Induced Mesomorphic Isotactic Polypropylene during Uniaxial Stretching at Different Temperatures. Polymer Crystallization, 2022, 2022, 1-13.	0.8	0
23	Constructing nickel chain/MXene networks in melamine foam towards phase change materials for thermal energy management and absorption-dominated electromagnetic interference shielding. Advanced Composites and Hybrid Materials, 2022, 5, 755-765.	21.1	105
24	Engineering hierarchical heterostructure material based on metal-organic frameworks and cotton fiber for high-efficient microwave absorber. Nano Research, 2022, 15, 6841-6850.	10.4	59
25	Multi-stimuli-responsive actuator based on bilayered thermoplastic film. Soft Matter, 2022, 18, 5052-5059.	2.7	8
26	Comparative study of the crystallization behavior and morphologies of carbon and glass fiber reinforced poly(ether ether ketone) composites. Polymers and Polymer Composites, 2021, 29, 1229-1239.	1.9	7
27	Effect of a small amount of poly(ethylene oxide) on crystal polymorphism of poly(l-lactic acid). Polymer Bulletin, 2021, 78, 6837-6846.	3.3	5
28	PAANa-induced ductile SEI of bare micro-sized FeS enables high sodium-ion storage performance. Science China Materials, 2021, 64, 105-114.	6.3	23
29	Facile Fabrication of Nylon66/Multi-Wall Carbon Nanotubes/Polyvinyl Alcohol Nanofiber Bundles for Use as Humidity Sensors. Journal of Macromolecular Science - Physics, 2021, 60, 368-380.	1.0	1
30	Recent Progress on the Alloyâ€Based Anode for Sodiumâ€Ion Batteries and Potassiumâ€Ion Batteries. Small, 2021, 17, e1903194.	10.0	284
31	An asymmetric sandwich structural cellulose-based film with self-supported MXene and AgNW layers for flexible electromagnetic interference shielding and thermal management. Nanoscale, 2021, 13, 2378-2388.	5.6	141
32	Improved microwave absorption performance of double helical C/Co@CNT nanocomposite with hierarchical structures. Journal of Materials Chemistry C, 2021, 9, 2178-2189.	5.5	49
33	Lightweight, Superelastic, and Hydrophobic Polyimide Nanofiber /MXene Composite Aerogel for Wearable Piezoresistive Sensor and Oil/Water Separation Applications. Advanced Functional Materials, 2021, 31, 2008006.	14.9	340
34	A resilient and lightweight bacterial cellulose-derived C/rGO aerogel-based electromagnetic wave absorber integrated with multiple functions. Journal of Materials Chemistry A, 2021, 9, 5566-5577.	10.3	62
35	Robust and efficient UV-reflecting one-dimensional photonic crystals enabled by organic/inorganic nanocomposite thin films for photoprotection of transparent polymers. Journal of Materials Chemistry C, 2021, 9, 4223-4232.	5.5	5
36	Flexible Transparent Polypyrrole-Decorated MXene-Based Film with Excellent Photothermal Energy Conversion Performance. ACS Applied Materials & Interfaces, 2021, 13, 8909-8918.	8.0	64

#	Article	IF	CITATIONS
37	Biodegradable PLA/CNTs/Ti3C2Tx MXene nanocomposites for efficient electromagnetic interference shielding. Journal of Materials Science: Materials in Electronics, 2021, 32, 25952-25962.	2.2	10
38	Flexible multilayered MXene/thermoplastic polyurethane films with excellent electromagnetic interference shielding, thermal conductivity, and management performances. Advanced Composites and Hybrid Materials, 2021, 4, 274-285.	21.1	237
39	Multifunctional Magnetic Ti ₃ C ₂ T _{<i>x</i>} MXene/Graphene Aerogel with Superior Electromagnetic Wave Absorption Performance. ACS Nano, 2021, 15, 6622-6632.	14.6	503
40	Ultraâ€High Initial Coulombic Efficiency Induced by Interface Engineering Enables Rapid, Stable Sodium Storage. Angewandte Chemie, 2021, 133, 11582-11587.	2.0	17
41	Environment Tolerant Conductive Nanocomposite Organohydrogels as Flexible Strain Sensors and Power Sources for Sustainable Electronics. Advanced Functional Materials, 2021, 31, 2101696.	14.9	179
42	Ultrathin flexible poly(vinylidene fluoride)/MXene/silver nanowire film with outstanding specific EMI shielding and high heat dissipation. Advanced Composites and Hybrid Materials, 2021, 4, 505-513.	21.1	190
43	Microribbon Structured Polyvinylidene Fluoride with High-Performance Piezoelectricity for Sensing Application. ACS Applied Polymer Materials, 2021, 3, 2411-2419.	4.4	15
44	Ultraâ€High Initial Coulombic Efficiency Induced by Interface Engineering Enables Rapid, Stable Sodium Storage. Angewandte Chemie - International Edition, 2021, 60, 11481-11486.	13.8	124
45	Superhydrophobic cellulose acetate/multiwalled carbon nanotube monolith with fiber cluster network for selective oil/water separation. Carbohydrate Polymers, 2021, 259, 117750.	10.2	33
46	Simultaneously improved solid particle erosion resistant and strength of graphene nanoplates/carbon nanotube enhanced thermoplastic polyurethane films. Journal of Applied Polymer Science, 2021, 138, 50924.	2.6	2
47	Versatile Janus Composite Nonwoven Solar Absorbers with Salt Resistance for Efficient Wastewater Purification and Desalination. ACS Applied Materials & Interfaces, 2021, 13, 24945-24956.	8.0	49
48	Electrostatic self-assembled NiFe2O4/Ti3C2Tx MXene nanocomposites for efficient electromagnetic wave absorption at ultralow loading level. Advanced Composites and Hybrid Materials, 2021, 4, 602-613.	21.1	97
49	Asymmetric Superhydrophobic Textiles for Electromagnetic Interference Shielding, Photothermal Conversion, and Solar Water Evaporation. ACS Applied Materials & Interfaces, 2021, 13, 28996-29007.	8.0	65
50	Tunable and Nacreâ€Mimetic Multifunctional Electronic Skins for Highly Stretchable Contactâ€Noncontact Sensing. Small, 2021, 17, e2100542.	10.0	69
51	Highly Thermal Conductive Poly(vinyl alcohol) Composites with Oriented Hybrid Networks: Silver Nanowire Bridged Boron Nitride Nanoplatelets. ACS Applied Materials & Interfaces, 2021, 13, 32286-32294.	8.0	67
52	Simple Approach to Fabricate an Anisotropic Wetting Surface with High Adhesive Force toward Droplet Transfer. ACS Applied Polymer Materials, 2021, 3, 4470-4477.	4.4	1
53	Synergistic Effect of Pressurization Rate and β-Form Nucleating Agent on the Multi-Phase Crystallization of iPP. Polymers, 2021, 13, 2984.	4.5	2
54	Bioinspired Multifunctional Photonicâ€Electronic Smart Skin for Ultrasensitive Health Monitoring, for Visual and Selfâ€Powered Sensing. Advanced Materials, 2021, 33, e2102332.	21.0	107

#	Article	IF	CITATIONS
55	Constructing dual thermal conductive networks in electrospun polyimide membranes with highly thermally conductivity but electrical insulation properties. Advanced Composites and Hybrid Materials, 2021, 4, 1102-1112.	21.1	47
56	Flexible Ag Microparticle/MXene-Based Film for Energy Harvesting. Nano-Micro Letters, 2021, 13, 201.	27.0	57
57	Ultra-stretchable and multifunctional wearable electronics for superior electromagnetic interference shielding, electrical therapy and biomotion monitoring. Journal of Materials Chemistry A, 2021, 9, 7238-7247.	10.3	65
58	Fire/heat-resistant, anti-corrosion and folding Ti ₂ C ₃ T _{<i>x</i>} MXene/single-walled carbon nanotube films for extreme-environmental EMI shielding and solar-thermal conversion applications. Journal of Materials Chemistry C, 2021, 9, 10425-10434.	5.5	45
59	Crystallization behavior of poly(lactic acid) and its blends. Polymer Crystallization, 2021, 4, e10171.	0.8	7
60	High-efficiency electromagnetic interference shielding capability of magnetic Ti ₃ C ₂ T _{<i>x</i>} MXene/CNT composite film. Journal of Materials Chemistry A, 2021, 9, 24560-24570.	10.3	68
61	Flexible Conductive Polyimide Fiber/MXene Composite Film for Electromagnetic Interference Shielding and Joule Heating with Excellent Harsh Environment Tolerance. ACS Applied Materials & Interfaces, 2021, 13, 50368-50380.	8.0	85
62	The Synergistic Effect of Rareâ€Earth Complex Nucleating Agent and Graphene Oxide on the Nonâ€Isothermal Crystallization Behavior of iPP Originating From the Diverse Selfâ€Assembly Morphology. Macromolecular Chemistry and Physics, 2021, 222, 2000357.	2.2	6
63	Influence of crystal orientation on stretching induced void formation in poly(4â€methylâ€1â€pentene) investigated by inâ€situ smallâ€angle and wideâ€angle <scp>Xâ€</scp> ray scattering. Polymer Crystallization, 2021, 4, e10215.	0.8	0
64	FeCo alloy nanoparticle decorated cellulose based carbon aerogel as a low-cost and efficient electromagnetic microwave absorber. Journal of Materials Chemistry C, 2021, 10, 126-134.	5.5	30
65	Self-Nucleation of β-Form Isotactic Polypropylene Lamellar Crystals in Thin Films. Macromolecules, 2021, 54, 11404-11411.	4.8	16
66	Highly Tunable Piezoelectricity of Flexible Nanogenerators Based on 3D Porously Architectured Membranes for Versatile Energy Harvesting and Self-Powered Multistimulus Sensing. ACS Sustainable Chemistry and Engineering, 2021, 9, 17128-17141.	6.7	15
67	Bimetal Synergistic Effect Induced High Reversibility of Conversion-Type Ni@NiCo ₂ S ₄ as a Free-Standing Anode for Sodium Ion Batteries. Journal of Physical Chemistry Letters, 2020, 11, 1435-1442.	4.6	54
68	Transparent Conductive Flexible Trilayer Films for a Deicing Window and Self-Recover Bending Sensor Based on a Single-Walled Carbon Nanotube/Polyvinyl Butyral Interlayer. ACS Applied Materials & Interfaces, 2020, 12, 1454-1464.	8.0	27
69	Selective dispersion of carbon nanotubes and nanoclay in biodegradable poly(ε-caprolactone)/poly(lactic acid) blends with improved toughness, strength and thermal stability. International Journal of Biological Macromolecules, 2020, 153, 1272-1280.	7.5	40
70	High-Performance Wearable Strain Sensor Based on Graphene/Cotton Fabric with High Durability and Low Detection Limit. ACS Applied Materials & Interfaces, 2020, 12, 1474-1485.	8.0	125
71	Simultaneously reinforcing and toughening poly(lactic acid) by incorporating reactive meltâ€functionalized silica nanoparticles. Journal of Applied Polymer Science, 2020, 137, 48834.	2.6	7
72	Temperature-dependent orientation of poly(ether ether ketone) under uniaxial tensile and its correlation with mechanical properties. Journal of Thermal Analysis and Calorimetry, 2020, 141, 1361-1369.	3.6	11

#	Article	IF	CITATIONS
73	Nucleation Mechanism for Form II to I Polymorphic Transformation in Polybutene-1. Macromolecules, 2020, 53, 6476-6485.	4.8	21
74	Fabrication of hierarchically porous superhydrophilic polycaprolactone monolith based on nonsolvent-thermally induced phase separation. RSC Advances, 2020, 10, 26319-26325.	3.6	13
75	An analytical model for temperature and crystalline evolution analysis of carbon fiber reinforced polymer composites during cooling. Polymer Composites, 2020, 41, 4074-4083.	4.6	1
76	Ultrafast printing of continuous fiberâ€reinforced thermoplastic composites with ultrahigh mechanical performance by ultrasonicâ€assisted laminated object manufacturing. Polymer Composites, 2020, 41, 4706-4715.	4.6	23
77	Mechanical, Thermal, and Rheological Properties of Ti ₃ C ₂ T _x MXene/ Thermoplastic Polyurethane Nanocomposites. Macromolecular Materials and Engineering, 2020, 305, 2000343.	3.6	44
78	Dewetting-Induced Alignment and Ordering of Cylindrical Mesophases in Thin Block Copolymer Films. Macromolecules, 2020, 53, 9631-9640.	4.8	6
79	Foaming Behaviors and Mechanical Properties of Injection-Molded Polylactide/Cotton-Fiber Composites. Industrial & Engineering Chemistry Research, 2020, 59, 17885-17893.	3.7	9
80	Flexible conductive MXene/cellulose nanocrystal coated nonwoven fabrics for tunable wearable strain/pressure sensors. Journal of Materials Chemistry A, 2020, 8, 21131-21141.	10.3	176
81	Flexible MXene/Silver Nanowire-Based Transparent Conductive Film with Electromagnetic Interference Shielding and Electro-Photo-Thermal Performance. ACS Applied Materials & Interfaces, 2020, 12, 40859-40869.	8.0	231
82	Shish–Kebab-Structured UHMWPE Coating for Efficient and Cost-Effective Oil–Water Separation. ACS Applied Materials & Interfaces, 2020, 12, 58252-58262.	8.0	18
83	Flexible conductive polymer composites for smart wearable strain sensors. SmartMat, 2020, 1, e1010.	10.7	119
84	Effects of Hydrothermal Aging of Carbon Fiber Reinforced Polycarbonate Composites on Mechanical Performance and Sand Erosion Resistance. Polymers, 2020, 12, 2453.	4.5	18
85	Cellulose acetate monolith with hierarchical micro/nano-porous structure showing superior hydrophobicity for oil/water separation. Carbohydrate Polymers, 2020, 241, 116361.	10.2	35
86	Effect of shear on nucleation of carbon fiber reinforced polymer composites: Experiments and modeling. Polymer Engineering and Science, 2020, 60, 2314-2323.	3.1	2
87	Achieving enhanced electromagnetic shielding and absorption capacity of cellulose-derived carbon aerogels <i>via</i> tuning the carbonization temperature. Journal of Materials Chemistry C, 2020, 8, 5191-5201.	5.5	51
88	Biodegradable poly(lactic acid) nanocomposites reinforced and toughened by carbon nanotubes/clay hybrids. International Journal of Biological Macromolecules, 2020, 151, 628-634.	7.5	66
89	Later Stage Melting of Isotactic Polypropylene. Macromolecules, 2020, 53, 2136-2144.	4.8	23
90	Ultrastable and Durable Silicone Coating on Polycarbonate Surface Realized by Nanoscale Interfacial Engineering. ACS Applied Materials & Interfaces, 2020, 12, 13296-13304.	8.0	17

#	Article	IF	CITATIONS
91	Modeling of Shear Rheological Behavior of Uncured Rubber Melt. Applied Rheology, 2020, 30, 130-137.	5.2	0
92	Crystallization behavior and mechanical properties of poly(lactic acid)/poly(ethylene oxide) blends nucleated by a self-assembly nucleator. Journal of Thermal Analysis and Calorimetry, 2019, 135, 3107-3114.	3.6	22
93	Structure and Mechanical Properties of Multi-Walled Carbon Nanotubes-Filled Isotactic Polypropylene Composites Treated by Pressurization at Different Rates. Polymers, 2019, 11, 1294.	4.5	6
94	Effect of different sterilization methods on the properties of commercial biodegradable polyesters for single-use, disposable medical devices. Materials Science and Engineering C, 2019, 105, 110041.	7.3	61
95	Relation Between Charge Transport and the Number of Interconnected Lamellar Poly(3-Hexylthiophene) Crystals. Macromolecules, 2019, 52, 6088-6096.	4.8	13
96	Ultraâ€Stretchable Porous Fiberâ€Shaped Strain Sensor with Exponential Response in Full Sensing Range and Excellent Antiâ€Interference Ability toward Buckling, Torsion, Temperature, and Humidity. Advanced Electronic Materials, 2019, 5, 1900538.	5.1	63
97	Facile and scalable synthesis of low-cost FeS@C as long-cycle anodes for sodium-ion batteries. Journal of Materials Chemistry A, 2019, 7, 19709-19718.	10.3	86
98	Highly Stretchable, Transparent, and Bioâ€Friendly Strain Sensor Based on Selfâ€Recovery Ionicâ€Covalent Hydrogels for Human Motion Monitoring. Macromolecular Materials and Engineering, 2019, 304, 1900227.	3.6	71
99	Poly(ethylene oxide)-promoted dispersion of graphene nanoplatelets and its effect on the properties of poly(lactic acid)/poly(butylene adipate-co-terephthalate) based nanocomposites. Materials Letters, 2019, 253, 34-37.	2.6	19
100	Highly Compressible and Robust Polyimide/Carbon Nanotube Composite Aerogel for High-Performance Wearable Pressure Sensor. ACS Applied Materials & Interfaces, 2019, 11, 42594-42606.	8.0	255
101	Superelastic and Durable Hierarchical Porous Thermoplastic Polyurethane Monolith with Excellent Hydrophobicity for Highly Efficient Oil/Water Separation. Industrial & Engineering Chemistry Research, 2019, 58, 20291-20299.	3.7	40
102	Ultrathin, flexible transparent Joule heater with fast response time based on single-walled carbon nanotubes/poly(vinyl alcohol) film. Composites Science and Technology, 2019, 183, 107796.	7.8	77
103	A Highly Sensitive and Stretchable Yarn Strain Sensor for Human Motion Tracking Utilizing a Wrinkle-Assisted Crack Structure. ACS Applied Materials & Interfaces, 2019, 11, 36052-36062.	8.0	141
104	Dynamic viscoelasticity and molecular orientation in uniaxially drawn PC/PET blends. Journal of Applied Polymer Science, 2019, 136, 47514.	2.6	4
105	Significant Stretchability Enhancement of a Crack-Based Strain Sensor Combined with High Sensitivity and Superior Durability for Motion Monitoring. ACS Applied Materials & Interfaces, 2019, 11, 7405-7414.	8.0	243
106	Superhydrophobic Electrically Conductive Paper for Ultrasensitive Strain Sensor with Excellent Anticorrosion and Self-Cleaning Property. ACS Applied Materials & Interfaces, 2019, 11, 21904-21914.	8.0	228
107	Anisotropic Conductive Polymer Composites Based on High Density Polyethylene/Carbon Nanotube/Polyoxyethylene Mixtures for Microcircuits Interconnection and Organic Vapor Sensor. ACS Applied Nano Materials, 2019, 2, 3636-3647.	5.0	30
108	Phase transitions of the rapidâ€compressionâ€induced mesomorphic isotactic polypropylene under highâ€pressure annealing. Journal of Polymer Science, Part B: Polymer Physics, 2019, 57, 651-661.	2.1	9

#	Article	IF	CITATIONS
109	Enhanced Solid Particle Erosion Properties of Thermoplastic Polyurethane arbon Nanotube Nanocomposites. Macromolecular Materials and Engineering, 2019, 304, 1900010.	3.6	53
110	Highâ€pressure induced formation of isotactic polypropylene mesophase: Synergistic effect of pressure and pressurization rate. Polymer Engineering and Science, 2019, 59, 439-446.	3.1	9
111	Facile Fabrication of Superhydrophobic and Eco-Friendly Poly(lactic acid) Foam for Oil–Water Separation via Skin Peeling. ACS Applied Materials & Interfaces, 2019, 11, 14362-14367.	8.0	132
112	Ultrasensitive and Highly Compressible Piezoresistive Sensor Based on Polyurethane Sponge Coated with a Cracked Cellulose Nanofibril/Silver Nanowire Layer. ACS Applied Materials & Interfaces, 2019, 11, 10922-10932.	8.0	331
113	Melting temperature, concentration and cooling rate-dependent nucleating ability of a self-assembly aryl amide nucleator on poly(lactic acid) crystallization. Polymer, 2019, 168, 77-85.	3.8	40
114	3D Viscoelastic Simulation of Jetting in Injection Molding. Polymer Engineering and Science, 2019, 59, E397.	3.1	4
115	Melt-Processed Poly(Ether Ether Ketone)/Carbon Nanotubes/Montmorillonite Nanocomposites with Enhanced Mechanical and Thermomechanical Properties. Materials, 2019, 12, 525.	2.9	22
116	Thermal Degradation Behavior and Kinetics of 3D Porous Polycarbonate Monoliths. Macromolecular Materials and Engineering, 2019, 304, 1800667.	3.6	10
117	Highâ€Performance Flexible Freestanding Anode with Hierarchical 3D Carbonâ€Networks/Fe ₇ S ₈ /Graphene for Applicable Sodiumâ€Ion Batteries. Advanced Materials, 2019, 31, e1806664.	21.0	233
118	Design of Helically Double-Leveled Gaps for Stretchable Fiber Strain Sensor with Ultralow Detection Limit, Broad Sensing Range, and High Repeatability. ACS Applied Materials & Interfaces, 2019, 11, 4345-4352.	8.0	91
119	Tunable temperature-resistivity behaviors of carbon black/polyamide 6 /high-density polyethylene composites with conductive electrospun PA6 fibrous network. Journal of Composite Materials, 2019, 53, 1897-1906.	2.4	8
120	A novel crystallization kinetics model of transcrystalline used for crystallization behavior simulation of short carbon fiberâ€reinforced polymer composites. Polymer Engineering and Science, 2019, 59, 854-862.	3.1	2
121	Competition effect of shearâ€induced nuclei and multiwalled carbon nanotubes (MWCNT) on βâ€isotactic polypropylene (<i>i</i> PP) formation in preshear injectionâ€molded <i>i</i> PP/MWCNT nanocomposites. Polymer Composites, 2018, 39, E1149.	4.6	6
122	The Cooperative Effect of Both Molecular and Supramolecular Chirality on Cell Adhesion. Angewandte Chemie, 2018, 130, 6585-6589.	2.0	17
123	The Cooperative Effect of Both Molecular and Supramolecular Chirality on Cell Adhesion. Angewandte Chemie - International Edition, 2018, 57, 6475-6479.	13.8	82
124	Systematic Control of Self-Seeding Crystallization Patterns of Poly(ethylene oxide) in Thin Films. Macromolecules, 2018, 51, 1626-1635.	4.8	26
125	An Alternating Skin–Core Structure in Melt Multiâ€Injectionâ€Molded Polyethylene. Macromolecular Materials and Engineering, 2018, 303, 1700465.	3.6	34
126	Superhydrophobic and superoleophilic porous reduced graphene oxide/polycarbonate monoliths for high-efficiency oil/water separation. Journal of Hazardous Materials, 2018, 344, 849-856.	12.4	122

#	Article	IF	CITATIONS
127	Continuously prepared highly conductive and stretchable SWNT/MWNT synergistically composited electrospun thermoplastic polyurethane yarns for wearable sensing. Journal of Materials Chemistry C, 2018, 6, 2258-2269.	5.5	376
128	Electrically conductive polymer composites for smart flexible strain sensors: a critical review. Journal of Materials Chemistry C, 2018, 6, 12121-12141.	5.5	522
129	Bioinspired Concentric-Cylindrical Multilayered Scaffolds with Controllable Architectures: Facile Preparation and Biological Applications. ACS Applied Materials & Interfaces, 2018, 10, 43512-43522.	8.0	20
130	Generating Nanoscopic Patterns in Conductivity within a Poly(3-hexylthiophene) Crystal via Bias-Controlled Scanning Probe Nanolithography. Macromolecules, 2018, 51, 7692-7698.	4.8	7
131	Facile Thermally Impacted Waterâ€Induced Phase Separation Approach for the Fabrication of Skinâ€Free Thermoplastic Polyurethane Foam and Its Recyclable Counterpart for Oil–Water Separation. Macromolecular Rapid Communications, 2018, 39, e1800635.	3.9	90
132	Ultrastretchable Multilayered Fiber with a Hollow-Monolith Structure for High-Performance Strain Sensor. ACS Applied Materials & Interfaces, 2018, 10, 34592-34603.	8.0	81
133	Superhydrophobic/Superoleophilic Polycarbonate/Carbon Nanotubes Porous Monolith for Selective Oil Adsorption from Water. ACS Sustainable Chemistry and Engineering, 2018, 6, 13747-13755.	6.7	198
134	Porous Polyethylene Bundles with Enhanced Hydrophobicity and Pumping Oil-Recovery Ability via Skin-Peeling. ACS Sustainable Chemistry and Engineering, 2018, 6, 12580-12585.	6.7	109
135	Shearâ€Induced Skinâ€Core Structure of Molten Isotactic Polypropylene and the Formation of βâ€Crystal. Macromolecular Materials and Engineering, 2018, 303, 1800083.	3.6	25
136	Aligned flexible conductive fibrous networks for highly sensitive, ultrastretchable and wearable strain sensors. Journal of Materials Chemistry C, 2018, 6, 6575-6583.	5.5	77
137	Ultra-stretchable, sensitive and durable strain sensors based on polydopamine encapsulated carbon nanotubes/elastic bands. Journal of Materials Chemistry C, 2018, 6, 8160-8170.	5.5	131
138	Facile Route to Improve the Crystalline Memory Effect: Electrospun Composite Fiber and Annealing. Macromolecular Chemistry and Physics, 2018, 219, 1800236.	2.2	11
139	Overview of the Experimental Trends in Waterâ€Assisted Injection Molding. Macromolecular Materials and Engineering, 2018, 303, 1800035.	3.6	26
140	Superhydrophobic Shish-kebab Membrane with Self-Cleaning and Oil/Water Separation Properties. ACS Sustainable Chemistry and Engineering, 2018, 6, 9866-9875.	6.7	147
141	Continuously fabricated transparent conductive polycarbonate/carbon nanotube nanocomposite films for switchable thermochromic applications. Journal of Materials Chemistry C, 2018, 6, 8360-8371.	5.5	79
142	Comparative assessment of the strain-sensing behaviors of polylactic acid nanocomposites: reduced graphene oxide or carbon nanotubes. Journal of Materials Chemistry C, 2017, 5, 2318-2328.	5.5	236
143	Pyrite FeS ₂ microspheres anchoring on reduced graphene oxide aerogel as an enhanced electrode material for sodium-ion batteries. Journal of Materials Chemistry A, 2017, 5, 5332-5341.	10.3	123
144	A tunable strain sensor based on a carbon nanotubes/electrospun polyamide 6 conductive nanofibrous network embedded into poly(vinyl alcohol) with self-diagnosis capabilities. Journal of Materials Chemistry C, 2017, 5, 4408-4418.	5.5	98

#	Article	IF	CITATIONS
145	Crystallization behavior of partially melted poly(ether ether ketone). Journal of Thermal Analysis and Calorimetry, 2017, 129, 1021-1028.	3.6	15
146	Crystallization behavior of poly(lactic acid) with a self-assembly aryl amide nucleating agent probed by real-time infrared spectroscopy and X-ray diffraction. Polymer Testing, 2017, 64, 12-19.	4.8	38
147	Simultaneous enhancements in the strength, modulus and toughness of electrospun polymeric membranes. RSC Advances, 2017, 7, 48054-48057.	3.6	5
148	Conductive Nanocomposites: Positive Temperature Coefficient (PTC) Evolution of Segregated Structural Conductive Polypropylene Nanocomposites with Visually Traceable Carbon Black Conductive Network (Adv. Mater. Interfaces 17/2017). Advanced Materials Interfaces, 2017, 4, .	3.7	0
149	Heating-induced negative temperature coefficient effect in conductive graphene/polymer ternary nanocomposites with a segregated and double-percolated structure. Journal of Materials Chemistry C, 2017, 5, 8233-8242.	5.5	66
150	Positive Temperature Coefficient (PTC) Evolution of Segregated Structural Conductive Polypropylene Nanocomposites with Visually Traceable Carbon Black Conductive Network. Advanced Materials Interfaces, 2017, 4, 1700265.	3.7	30
151	Morphological Changes of Isotactic Polypropylene Crystals Grown in Thin Films. Macromolecules, 2017, 50, 6210-6217.	4.8	25
152	A Prerequisite of the Poly(εâ€Caprolactone) Selfâ€Induced Nanohybrid Shish–Kebab Structure Formation: An Ordered Crystal Lamellae Orientation Morphology of Fibers. Macromolecular Chemistry and Physics, 2017, 218, 1700414.	2.2	11
153	Flexible and Lightweight Pressure Sensor Based on Carbon Nanotube/Thermoplastic Polyurethane-Aligned Conductive Foam with Superior Compressibility and Stability. ACS Applied Materials & Interfaces, 2017, 9, 42266-42277.	8.0	225
154	A flexible and self-formed sandwich structure strain sensor based on AgNW decorated electrospun fibrous mats with excellent sensing capability and good oxidation inhibition properties. Journal of Materials Chemistry C, 2017, 5, 7035-7042.	5.5	100
155	Hydrophobic polycarbonate monolith with mesoporous nest-like structure: an effective oil sorbent. Materials Letters, 2017, 188, 201-204.	2.6	34
156	Lightweight conductive graphene/thermoplastic polyurethane foams with ultrahigh compressibility for piezoresistive sensing. Journal of Materials Chemistry C, 2017, 5, 73-83.	5.5	576
157	Simulation of Jetting in Injection Molding Using a Finite Volume Method. Polymers, 2016, 8, 172.	4.5	10
158	Simultaneously improving tensile strength and toughness of meltâ€spun βâ€nucleated isotactic polypropylene fibers. Journal of Applied Polymer Science, 2016, 133, .	2.6	5
159	Numerical simulation for flowâ€induced stress in injection/compression molding. Polymer Engineering and Science, 2016, 56, 287-298.	3.1	10
160	CdS nanorods/organic hybrid LED array and the piezo-phototronic effect of the device for pressure mapping. Nanoscale, 2016, 8, 8078-8082.	5.6	78
161	Organic vapor sensing behaviors of conductive thermoplastic polyurethane–graphene nanocomposites. Journal of Materials Chemistry C, 2016, 4, 4459-4469.	5.5	198
162	Carbon Nanotubes-Adsorbed Electrospun PA66 Nanofiber Bundles with Improved Conductivity and Robust Flexibility. ACS Applied Materials & Interfaces, 2016, 8, 14150-14159.	8.0	241

#	Article	IF	CITATIONS
163	Annealing Induced Mechanical Reinforcement of Injection Molded iPP Parts. Macromolecular Materials and Engineering, 2016, 301, 1468-1472.	3.6	38
164	CdS@SiO ₂ Core-Shell Electroluminescent Nanorod Arrays Based on a Metal-Insulator-Semiconductor Structure. Small, 2016, 12, 5734-5740.	10.0	14
165	Liquid-sensing behaviors of carbon black/polyamide 6/high-density polyethylene composite containing ultrafine conductive electrospun fibrous network. Colloid and Polymer Science, 2016, 294, 1343-1350.	2.1	8
166	Mechanically Strengthened Polyamide 66 Nanofibers Bundles via Compositing With Polyvinyl Alcohol. Macromolecular Materials and Engineering, 2016, 301, 212-219.	3.6	12
167	Effects of surface modification with 3â€aminopropyltriethoxysilane on structure and mechanical property of multiwalled carbon nanotube/polycarbonate composites. Polymer Composites, 2016, 37, 1914-1923.	4.6	11
168	Electrically conductive thermoplastic elastomer nanocomposites at ultralow graphene loading levels for strain sensor applications. Journal of Materials Chemistry C, 2016, 4, 157-166.	5.5	484
169	Microstructure and Mechanical Properties of Isotactic Polypropylene Films Fabricated via Melt-Extrusion and Uniaxial-Stretching. Journal of Macromolecular Science - Physics, 2016, 55, 158-174.	1.0	6
170	Cold crystallization behavior of glassy poly(lactic acid) prepared by rapid compression. Polymer Engineering and Science, 2015, 55, 359-366.	3.1	13
171	Tailoring microstructure and mechanical properties of injection molded isotactic–polypropylene via high temperature preshear. Polymer Engineering and Science, 2015, 55, 2714-2721.	3.1	9
172	Morphology evolution for isotactic polypropylene: Experiment and simulation. Polymer Science - Series A, 2015, 57, 552-564.	1.0	1
173	A facile strategy for functionalizing silica nanoparticles by polycarbonate degradation and its application in polymer nanocomposites. Polymer Degradation and Stability, 2015, 119, 295-298.	5.8	16
174	Evaluation of typical rheological models fitting for polycarbonate squeeze flow. Journal of Applied Polymer Science, 2015, 132, .	2.6	1
175	Fabrication of a polymer/aligned shish-kebab composite: microstructure and mechanical properties. RSC Advances, 2015, 5, 60392-60400.	3.6	12
176	Suppressing the skin–core structure in injection-molded HDPE parts via the combination of pre-shear and UHMWPE. RSC Advances, 2015, 5, 84483-84491.	3.6	15
177	Twoâ€stage drawing process to prepare highâ€strength and porous ultrahighâ€molecularâ€weight polyethylene fibers: Cold drawing and hot drawing. Journal of Applied Polymer Science, 2015, 132, .	2.6	15
178	New insight into lamellar branching of β-nucleated isotactic polypropylene upon melt-stretching: WAXD and SAXS study. Journal of Materials Science, 2015, 50, 599-604.	3.7	25
179	Liquidâ€sensing behaviors of carbon black/polypropylene and carbon nanotubes/polypropylene composites: A comparative study. Polymer Composites, 2015, 36, 205-213.	4.6	8
180	Nonisothermal Crystallization Kinetics of Poly(lactic acid) Nucleated with a Multiamide Nucleating Agent. Journal of Macromolecular Science - Physics, 2014, 53, 1680-1694.	1.0	31

#	Article	IF	CITATIONS
181	Study on Impact Property and Fracture Morphology of Injection-molded Optical-grade Polycarbonate. Journal of Macromolecular Science - Physics, 2014, 53, 336-346.	1.0	1
182	Preparation and Characterization of a Bipolar Membrane Modified by Copper Phthalocyanine 16-Carboxylic Acid and Acetyl Ferrocene. Journal of Macromolecular Science - Physics, 2014, 53, 1431-1441.	1.0	8
183	The strain-sensing behaviors of carbon black/polypropylene and carbon nanotubes/polypropylene conductive composites prepared by the vacuum-assisted hot compression. Colloid and Polymer Science, 2014, 292, 945-951.	2.1	18
184	Wide distribution of shish-kebab structure and tensile property of micro-injection-molded isotactic polypropylene microparts: a comparative study with injection-molded macroparts. Journal of Materials Science, 2014, 49, 1041-1048.	3.7	36
185	Effects of modified silica on morphology, mechanical property, and thermostability of injection-molded polycarbonate/silica nanocomposites. Journal of Reinforced Plastics and Composites, 2014, 33, 911-922.	3.1	16
186	Thermal degradation mechanism and kinetics of polycarbonate/silica nanocomposites. Polymer Degradation and Stability, 2014, 107, 129-138.	5.8	68
187	One-pot synthesis and the electrochemical properties of nano-structured nickel selenide materials with hierarchical structure. CrystEngComm, 2013, 15, 2624.	2.6	24
188	The degradation rate of polyanhydride (poly(sebacic acid), diacetoxy terminated, PSADT). Journal Wuhan University of Technology, Materials Science Edition, 2013, 28, 793-797.	1.0	8
189	Crystallization of poly(lactic acid) enhanced by phthalhydrazide as nucleating agent. Polymer Bulletin, 2013, 70, 2911-2922.	3.3	27
190	Organic vapor sensing behaviors of carbon black/poly (lactic acid) conductive biopolymer composite. Colloid and Polymer Science, 2013, 291, 2871-2878.	2.1	28
191	Crystallization of poly(lactic acid) accelerated by cyclodextrin complex as nucleating agent. Polymer Bulletin, 2013, 70, 195-206.	3.3	59
192	β-Crystal in the iPP melt encapsulated by transcrystallinity and spherulites: effect of molecular weight. Journal of Materials Science, 2013, 48, 2326-2333.	3.7	3
193	Unexpected molecular weight dependence of shish kebab in waterâ€assisted injection molded HDPE. Polymers for Advanced Technologies, 2013, 24, 270-272.	3.2	21
194	Enhanced βâ€crystal formation of isotactic polypropylene under the combined effects of acidâ€corroded glass fiber and preshear. Polymer Composites, 2013, 34, 1250-1260.	4.6	15
195	Enhancing particle erosion resistance of glassâ€reinforced polymeric composites using carbon nanofiberâ€based nanopaper coatings. Journal of Applied Polymer Science, 2013, 129, 1875-1881.	2.6	14
196	Effect of Rapid Compression on the Crystallization Behaviour of Polyethylene. Polymers and Polymer Composites, 2013, 21, 543-552.	1.9	0
197	Effect of Shear Stress on Crystallization of Isotactic Polypropylene from a Structured Melt. Macromolecules, 2012, 45, 8933-8937.	4.8	60
198	Scale effect on filling stage in micro-injection molding for thin slit cavities. Microsystem Technologies, 2012, 18, 2085-2091.	2.0	16

#	Article	IF	CITATIONS
199	Three-dimensional CuS hierarchical architectures as recyclable catalysts for dye decolorization. CrystEngComm, 2012, 14, 3965.	2.6	77
200	Large-scale stereoscopic structured heazlewoodite microrod arrays and scale-like microsheets for lithium-ion battery applications. RSC Advances, 2012, 2, 6817.	3.6	29
201	Effect of Stretching on <i>β</i> -Phase Content of Isotactic Polypropylene Melt Containing <i>β</i> -Nucleating Agent. Journal of Macromolecular Science - Physics, 2012, 51, 828-838.	1.0	4
202	Preparation and characterization of microbial biodegradable poly(3â€hydroxybutyrateâ€ <i>co</i> â€4â€hydroxybutyrate)/organoclay nanocomposites. Polymer Composites, 2012, 33, 838-842.	4.6	17
203	Enhanced orientation of the waterâ€assisted injectionâ€molded ipp in the presence of nucleating agent. Polymer Engineering and Science, 2012, 52, 725-732.	3.1	22
204	The hierarchical structure of waterâ€assisted injection molded high density polyethylene: Small angle Xâ€ray scattering study. Journal of Applied Polymer Science, 2012, 125, 2297-2303.	2.6	19
205	Transcrystallization in nanofiber bundle/isotactic polypropylene composites: effect of matrix molecular weight. Colloid and Polymer Science, 2012, 290, 1157-1164.	2.1	14
206	Inhomogeneous deformation of crystalline skeleton of syndiotactic polypropylene under uniaxial stretching. Journal of Materials Science, 2012, 47, 3334-3343.	3.7	9
207	Morphological comparison of isotactic polypropylene molded by water-assisted and conventional injection molding. Journal of Materials Science, 2011, 46, 7830-7838.	3.7	39
208	HDPE solution crystallization induced by electrospun PA66 nanofiber. Colloid and Polymer Science, 2011, 289, 843-848.	2.1	13
209	Crystal modifications and multiple melting behavior of poly(<scp>L</scp> ″actic) Tj ETQq1 1 0.784314 rgBT /Ov 409-413.	verlock 10 2.1	Tf 50 347 To 32
210	Negative effect of stretching on the development of βâ€phase in βâ€nucleated isotactic polypropylene. Polymer International, 2011, 60, 1016-1023.	3.1	9
211	Oriented structure in stretched isotactic polypropylene melt and its unexpected recrystallization: optical and Xâ€ray studies. Polymer International, 2011, 60, 1434-1441.	3.1	17
212	Crystal morphology and structure of the βâ€form of isotactic polypropylene under supercooled extrusion. Journal of Applied Polymer Science, 2011, 120, 3255-3264.	2.6	18
213	Optimization of runner sizes and process conditions considering both part quality and manufacturing cost in injecting molding. Journal of Polymer Engineering, 2011, 31, .	1.4	1
214	Competing effect of shear and β-nucleating agent on the crystallization of injection-molded iPP. E-Polymers, 2010, 10, .	3.0	0
215	Response of Two-Dimensional Polymeric Cadmium Ferrocenyl Disulfonates to Heavy Metal Ions. Journal of Inorganic and Organometallic Polymers and Materials, 2010, 20, 847-855.	3.7	2
216	Zinc Coordination Complex for use in Uniform ZnS Microflowers Synthesis. Zeitschrift Fur Anorganische Und Allgemeine Chemie, 2010, 636, 1913-1916.	1.2	0

#	Article	IF	CITATIONS
217	Nonisothermal crystallization kinetics of poly(lactic acid) formulations comprising talc with poly(ethylene glycol). Polymer Engineering and Science, 2010, 50, 2298-2305.	3.1	72
218	The Numerical Simulation of the Crystallization Morphology Evolution of Semi-Crystalline Polymers in Injection Molding. Polymer-Plastics Technology and Engineering, 2010, 49, 1036-1048.	1.9	11
219	Self-assembly of a Sandwich-like Cadmium Ferrocenyl Coordination Polymer and its Third-Order Nonlinear Optical Properties. Synthesis and Reactivity in Inorganic, Metal Organic, and Nano Metal Chemistry, 2010, 40, 725-728.	0.6	7
220	Suppression of β-crystal in iPP/PET Fiber Composites. Polymer-Plastics Technology and Engineering, 2010, 49, 154-157.	1.9	8
221	Skin Thickness and β-Crystals Development in Injection-Molded iPP Along the Flow Direction. Journal of Macromolecular Science - Physics, 2009, 48, 439-448.	1.0	3
222	Computing flow-induced stresses of injection molding based on the Phan–Thien–Tanner model. Archive of Applied Mechanics, 2008, 78, 363-377.	2.2	17
223	Transcrystallinity in a Polycarbonate(PC)/Polyethylene(PE) Blend Prepared by Gas-Assisted Injection Molding: A New Understanding of Its Formation Mechanism. Journal of Macromolecular Science - Physics, 2008, 47, 829-836.	1.0	7
224	Effects of Process Parameters and Two-Way Interactions on Sink Mark Depth of Injection Molded Parts by Using the Design of Experiment Method. Polymer-Plastics Technology and Engineering, 2007, 47, 30-35.	1.9	9
225	Investigation of the Effect of Molding Variables on Sink Marks of Plastic Injection Molded Parts Using Taguchi DOE Technique. Polymer-Plastics Technology and Engineering, 2007, 46, 219-225.	1.9	34
226	Optimization for Injection Molding Process Conditions of the Refrigeratory Top Cover Using Combination Method of Artificial Neural Network and Genetic Algorithms. Polymer-Plastics Technology and Engineering, 2007, 46, 105-112.	1.9	14
227	Preparation of SiC–SiO2–CuO composites. Journal of Materials Science, 2007, 42, 7457-7460.	3.7	6
228	Nonisothermal melt crystallization kinetics of poly(ethylene terephthalate)/clay nanocomposites. Journal of Applied Polymer Science, 2004, 91, 308-314.	2.6	91
229	Nonisothermal Cold Crystallization Kinetics of Poly(ethylene terephthalate)/Clay Nanocomposite. Polymer Journal, 2003, 35, 884-889.	2.7	17